PCCP

Structure and infrared (IR) assignments for the OLED material: *N*,*N*′-diphenyl-*N*,*N*′-bis(1-naphthyl)-1,1′-biphenyl-4,4″-diamine (NPB)†

Mathew D. Halls,[a] Carl P. Tripp*[b] and H. Bernhard Schlegel*[a]

[a] *Department of Chemistry, Wayne State University, Detroit MI 48202, USA. E-mail: hbs@chem.wayne.edu*
[b] *Department of Chemistry and LASST, University of Maine, Orono ME 04469, USA. E-mail: ctripp@maine.maine.edu*

Received 19th February 2001, Accepted 12th April 2001
First published as an Advance Article on the web 10th May 2001

Organic light-emitting diodes (OLEDs) are currently under intense investigation for use in next-generation display technologies. Research into the fundamental properties of the materials used in OLEDs, such as structure and vibrational modes, will help provide experimental probes which are required to gain insight into the processes leading to device degradation and failure. Calculations using the hybrid B3LYP functional and the split-valence polarized 6-31G(d) basis set have been carried out to assign the IR bands of the OLED hole transport material *N*,*N*′-diphenyl-*N*,*N*′-bis(1-naphthyl)-1,1′-biphenyl-4,4″-diamine (NPB). Excellent agreement was found between the computed and experimental wavenumbers allowing the reliable assignment of major IR bands. Comparison of the reflection absorption IR (RAIRS) spectra obtained from room temperature and thermally annealed NPB thin films indicates that, upon annealing, structural changes occur and the average orientation of the NPB naphthyl groups become predominately flat with respect to the surface.

Introduction

Following the initial report, by Tang and Van Slyke,[1] organic light-emitting diodes (OLEDs) have received widespread attention for their potential use in next-generation display technologies.[2,3] OLEDs are typically amorphous thin solid film heterojunction devices constructed by vacuum evaporation of the transport layers onto a supporting electrode. The organic materials composing the active layers are chosen with close regard to their relative orbital energy offsets, usually such that exciton formation and recombination occurs in the electron transport layer of the device. Materials development for electron transport and emission in OLEDs has largely focused on metallo-quinolates,[4,5] with tris(8-hydroxyquinoline)-aluminium(III) (Alq3) being the most often used. Aromatic amines are often used as hole transport materials in OLED devices and have had good success. In particular, the naphthyl diamine *N*,*N*′-diphenyl-*N*,*N*′-bis(1-naphthyl)-1,1′-biphenyl-4,4″ -diamine (NPB) was shown, by Tang and coworkers,[6] to afford improved stability over previously used amines.

Although showing excellent device characteristics, OLEDs still suffer from a lack of long-term device stability. Numerous causes of device degradation have been proposed in the literature, including the delamination of electrodes,[7] cathode oxidation,[8] electrochemical reactions at electrode/organic interfaces,[9] hydrolysis of the metallo-quinolate layer,[10] and an intrinsic instability of the metallo-quinolate cation.[11] Device failure has also been attributed to crystallization of the active layers, especially the hole transport layer.[12]

Despite the importance of the archetype hole transport molecule NPB, relatively few studies of its fundamental molecular properties have appeared in the literature. Theoretical investigations into the electronic density of states and the effect of charging on the electronic structure of NPB were reported by Lee and co-workers.[13,14] The hole transport mobility of NPB was measured by Deng *et al.*[15] using the time of flight technique. Also Tang and co-workers[16] have studied the growth models of NPB on ITO substrates using AFM.

Infrared (IR) spectroscopy is a standard tool for structural characterization and following the evolution and dynamics of chemical systems. The infrared assignments of NPB have not yet been reported. For large molecules, quantum chemical calculations predicting harmonic frequencies and spectral intensities are essential when interpreting experimental IR spectra, where the high density of states results in spectral complexity in the region below *ca.* 1700 cm^{-1}. The availability of analytical geometric and electric field derivatives,[17] coupled with advances in computer performance has extended the applicability of electronic structure methods to systems as large as NPB. In the theoretical prediction of molecular vibrational properties, density functional theory (DFT) has been demonstrated to be a cost-effective alternative to conventional *ab initio* approaches, significantly outperforming methods such as Hartree–Fock and second-order Møller–Plesset perturbation theory (MP2).[18–20]

In the present work, the equilibrium geometry, vibrational frequencies and IR intensities for NPB are computed using hybrid DFT and a medium sized split-valence basis set to enable the assignment of major bands in the experimental pellet IR spectrum. The observed IR bands are assigned on the basis of the frequency agreement and IR intensity patterns between the theoretical and observed spectra and visualization of computer normal mode displacement vectors. Using the NPB IR assignments, a comparison of the surface IR spectra, obtained from room temperature and thermally

† Electronic Supplementary Information available. See http://www.rsc.org/suppdata/cp/b1/b101619i/

annealed NPB thin films, provides insight into the conformational changes arising upon annealing.

Methods

N,*N*′-diphenyl-*N*,*N*′-bis(1-naphthyl)-1,1′-biphenyl-4,4″-diamine (NPB) was obtained from the Xerox Research Center Canada (XRCC). The transmission IR spectrum was recorded from isotropically dispersed NPB in KBr. The IR spectrum was collected over the spectral region 400 cm^{-1} to 4000 cm^{-1} on a Bomem 102 FT-IR equipped with a CsI beamsplitter and a DTGS detector with 4 cm^{-1} resolution. To examine the spectral changes in thin solid films upon thermal annealing, a thin solid film of NPB was deposited onto a silver mirror. The silver was thermally evaporated on a glass slide to a total mass thickness of 1000 Å using a standard vacuum system evaporator operating at a background pressure of 10^{-6} Torr. The NPB was deposited onto the Ag/glass substrate to a total mass thickness of 200 Å using a second vacuum system evaporator. Reflection absorption IR spectra (RAIRS) were collected from the thin solid film using the Bomem 102 FT-IR equipped with a Spectra-Tech FT-80 grazing angle accessory fixed at 80°. The RAIRS spectrum of the NPB thin film was recorded at room temperature and after annealing at 125 °C for 30 min, for comparison.

The theoretical results reported here were obtained using the GAUSSIAN 98 suite of programs.[21] The geometry of NPB was optimized and harmonic frequencies and IR intensities were computed using the hybrid B3LYP density functional, corresponding to the combination of the Becke's three-parameter exchange functional (B3)[22] with the Lee–Yang–Parr fit for electron correlation (LYP),[23] along with the polarized split-valence basis set 6-31G(d) (which provides a total of 754 basis functions for NPB).[24]

Results and discussion

Structure and molecular vibrations of NPB

The molecular structure of NPB along with the pellet IR spectrum is shown in Fig. 1. NPB is composed of terminal phenyl amines with naphthyl moieties joined by a bridging biphenyl group. The naphthyl groups in NPB give rise to a number of structural conformations, which may be present in the solid state. The gas phase geometry of NPB was optimized at the B3LYP/6-31G(d) level of theory without symmetry constraints (C_1) starting from a structure that corresponds to the global minimum, as calculated by a semiempirical PM3 molecular orbital study by other authors.[14] The optimized structure of NPB is determined to have a point of symmetry at the central CC bond in the biphenyl bridge in agreement with the previous semiempirical calculations. A table of calculated heavy atom bond lengths of NPB along with experimental data for smaller molecules representative of the fragments composing NPB (1-aminonaphthalene, aniline and 1,1′-biphenyl-4,4′-diamine (benzidine)) is available (see ESI Table S1).†

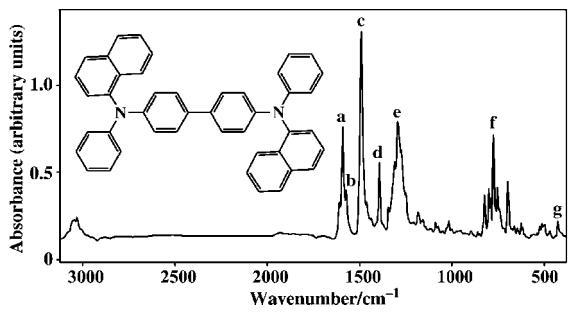

Fig. 1 Molecular structure of NPB and the IR spectrum from isotropically dispersed NPB in KBr. Characteristic IR bands are labelled (**a**–**g**).

NPB is composed of 78 atoms giving rise to 228 vibrational degrees of freedom. To allow interpretation of the experimental pellet IR spectrum, harmonic vibrational frequencies, corresponding normal modes and IR intensities computed in the double harmonic approximation ($I_{IR} \propto |\partial\mu/\partial Q_k|^2$) were calculated. Work in our laboratory has demonstrated that the hybrid B3LYP functional predicts IR intensities in close agreement with those calculated with the conventional highly correlated *ab initio* method quadratic configuration interaction including singly and doubly excited determinants (QCISD).[20] In particular, the B3LYP/6-31G(d) level of theory represents a cost effective choice for the calculation of theoretical IR spectra, particularly for large molecules such as NPB. The calculated vibrational frequencies are all real, verifying that the optimized geometry is a true minimum on the potential energy surface. A complete table of theoretical harmonic frequencies and IR intensities for NPB is available (see ESI Table S2).†

Theoretical harmonic frequencies typically overestimate observed fundamentals due to the neglect of mechanical anharmonicity, electron correlation and basis set effects. To compensate, various scaling strategies exist to bring the computed harmonics into greater agreement with experiment.[18,19,25–28] Studies by Scott and Radom,[18] and Wong[19] have shown that B3LYP calculations employing the 6-31G(d) basis set provides harmonic frequencies that can be effectively scaled for comparison with experimental wavenumbers. In this work, to improve the agreement with experiment, the B3LYP/6-31G(d) harmonic frequencies were scaled by a factor of 0.97 as discussed below.

To compare with the experimental results, a simulated IR spectrum was constructed using the scaled theoretical vibrational frequencies and computed intensities by representing the IR bands by Gaussian lineshapes with a full width at half maximum (FWHM) of 4 cm^{-1}. The vibrational spectra of complex molecules are usually discussed in terms of different wavenumber regions known to generally correspond to different types of vibrational modes. The upper wavenumber region (*ca.* 3600 cm^{-1} to 1700 cm^{-1}) contains vibrations composed largely of localised hydrogen stretches, whereas the mid-wavenumber region (*ca.* 1700 cm^{-1} to 1000 cm^{-1}) contains heavy atom in-plane stretches and bends, and the low-wavenumber region (below 1000 cm^{-1}), the out-of-plane and torsional modes. It is in the latter two regions, below 1700 cm^{-1} (the fingerprint region), where quantum chemical prediction can be the most useful in making vibrational band assignments that may not otherwise be interpretable. The experimental pellet IR spectrum for NPB consists of two groups of bands having substantial intensity as seen in Fig. 1. The simulated and the experimental IR spectra for these two regions are expanded and compared in Fig. 2. The agreement between the simulated and experimental IR spectra is excellent, allowing reliable correlation between theoretically predicted and experimentally observed bands.

In-plane region assignments

The top panel in Fig. 2 presents the first spectral range of substantial intensity, from *ca.* 1150 cm^{-1} to 1650 cm^{-1}, which generally contains heavy atom in-plane stretches and bends. The experimental and theoretical frequencies and general mode assignments for observed IR bands in the in-plane region are given in Table 1. The band assignments were made on the basis of frequency and intensity pattern agreement and the description from visualisation of the atomic displacement vectors. The most intense bands in this region are denoted in Fig. 1 and Table 1 with letters **a**, **c**, **d** and **e**. The band marked **a** at 1592 cm^{-1} in the experimental spectrum is assigned to a CC stretching vibration largely involving the terminal phenyl groups (t-phenyl), predicted to have a frequency of 1606 cm^{-1}.

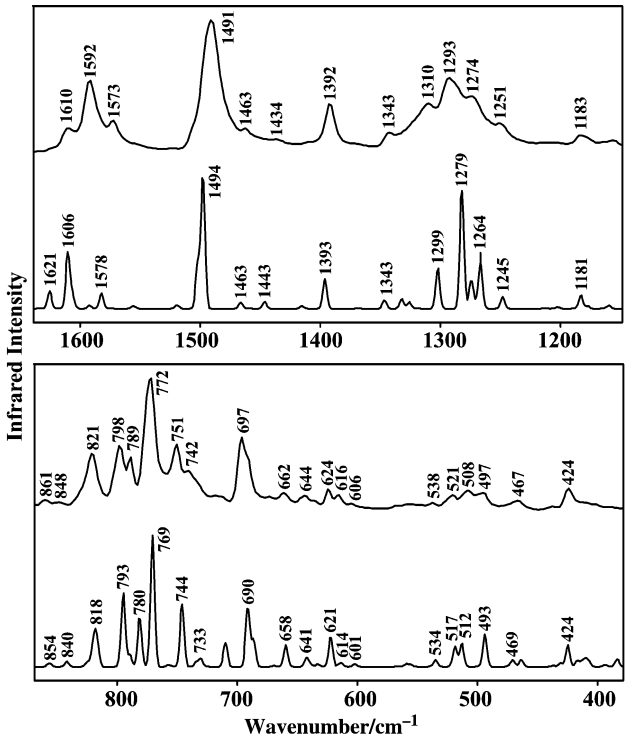

Fig. 2 Experimental IR spectrum and the B3LYP/6-31G(d) simulated IR spectrum of the in-plane region (top panel) and the out-of-plane region (bottom panel) for comparison.

This is comparable to the CC stretching vibration of aniline observed at 1604 cm^{-1} in the liquid phase and calculated to be 1608 cm^{-1} using scaled B3LYP/6-31G(d).[29] Although it is less intense than the other bands discussed here, the vibration marked **b** in Fig. 1 and Table 1 at 1573 cm^{-1} is notable, since it is assigned as a naphthyl CC stretching mode computed at 1578 cm^{-1}. The **c** band observed at 1491 cm^{-1} is predicted at 1494 cm^{-1} and corresponds to a CC/CN stretching + CH bending vibration associated with both the terminal and bridging phenyl groups in NPB. The **d** vibration at 1392 cm^{-1} is predicted to occur at 1393 cm^{-1} and involves CC/CN stretching + CH bending of the naphthyl moieties of NPB. An envelope of overlapping bands is observed in the experimental IR with an obvious peak with maximum intensity at 1293 cm^{-1}, labelled **e**. The **e** band is computed at 1279 cm^{-1} and is attributed to a CH/CCN bending + CN stretching vibration involving the terminal and bridging phenyl groups.

Out-of-plane region assignments

The bottom panel of Fig. 2 shows the second intense region, from *ca.* 860 cm^{-1} to 400 cm^{-1}, which generally contains out-of-plane vibrational modes. The experimental and theoretical wavenumbers and general mode assignments for observed IR bands in the out-of-plane region are given in Table 2. The most intense absorption in this wavenumber region is denoted **f** in Fig. 1 and Table 2 and is observed at 772 cm^{-1}. This band is computed to have a frequency of 769 cm^{-1} and is assigned to the out-of-plane CH wag of the naphthyl groups of NPB. This band is comparable to that computed at 767 cm^{-1} for 1-aminonaphthalene using the scaled B3LYP/4-31G level of theory, as reported recently by Bauschlicher.[30] The band marked **g**, observed at 424 cm^{-1} in the experimental spectrum, corresponds to a naphthyl CC torsion vibration, predicted at 424 cm^{-1}.

Agreement between scaled harmonic frequencies and experiment

Theoretical harmonic frequencies are often scaled to compare with experimental wavenumbers. The scaling factor employed in the present study of 0.97 is comparable to the scaling factor suggested by Scott and Radom of 0.9614.[18] The average absolute difference, average difference and standard deviation between the theoretical and experimental frequencies for the assignments presented here are *ca.* 25 cm^{-1}, 25 cm^{-1} and 14 cm^{-1}, respectively. After scaling, the agreement improves significantly, giving an average absolute difference, average difference and standard deviation of *ca.* 6 cm^{-1}, −4 cm^{-1} and 6 cm^{-1}. Unscaled B3LYP/6-31G(d) harmonic frequencies show a tendency to overestimate experimental fundamentals, with a large number of frequencies overestimating the experimental data by more than 50 cm^{-1}. After scaling, the error distribution is much more favourable, being peaked at zero difference (see ESI† Fig. S1 for $\nu_{calc} - \nu_{expt}$ histogram). The raw B3LYP/6-31G(d) frequencies are included in Tables 1 and 2 for individual comparison with the scaled and experimentally observed wavenumbers.

Table 1 Experimental and B3LYP/6-31G(d) calculated frequencies, and general mode assignments for observed IR bands in the in-plane region of the spectrum

	B3LYP/6-31G(d)/cm^{-1}	Scaled[a]/cm^{-1}	Observed/cm^{-1}	Assignment[b]
	1671	1621	1610	CC stretch (biphenyl)
a	1656	1606	1592	CC stretch (t-phenyl)
b	1627	1578	1573	CC stretch (naphthyl)
	1545	1498	1504 sh	CC stretch + CH bend (phenyl)
c	1540	1494	1491	CC stretch + CH bend + CN stretch (phenyl)
	1508	1463	1463	CC stretch + CH bend + CN stretch (naphthyl)
	1487	1443	1434	CC stretch + CH bend (naphthyl)
d	1436	1393	1392	CC stretch + CH bend + CN stretch (naphthyl)
	1385	1343	1343	CC bend (naphthyl)
	1339	1299	1310	CH bend + CH stretch + CCN bend (phenyl)
e	1319	1279	1293	CH bend + CN stretch + CCN bend (phenyl)
	1303	1264	1274	CC stretch + CH bend + CN stretch
	1284	1245	1251	CC stretch + CH bend + CN stretch (naphthyl)
	1217	1181	1183	CH bend + CN stretch (biphenyl)
	1193	1157	1156	CH bend + CC stretch (naphthyl)
	1119	1086	1087	CH bend + CC stretch (t-phenyl + naphthyl)
	1110	1077	1074	CH bend + CC stretch (t-phenyl + naphthyl)
	1078	1046	1051	CH bend + CC deformation
	1056	1025	1028	Ring deformation
	1050	1019	1015	Ring deformation
	1017	986	1001	Ring deformation (biphenyl)

[a] Harmonic frequencies were scaled by 0.97. [b] Terminal phenyl groups are indicated by 't-phenyl'.

Table 2 Experimental and B3LYP/6-31G(d) calculated frequencies, and general mode assignments for observed IR bands in the out-of-plane region of the spectrum

	B3LYP/6-31G(d)/cm^{-1}	Scaled[a]/cm^{-1}	Observed/cm^{-1}	Assignment
	975	946	966	CH wag (naphthyl)
	962	933	953	CH wag
	914	887	896	CH wag (naphthyl)
	881	854	861	CH wag (naphthyl)
	866	840	848	CH wag (biphenyl)
	840, 842, 843	815, 816, 818	821	CH wag (phenyl)
	818	793	798	CH wag (naphthyl)
	804	780	789	CH wag + CC deformation (naphthyl + t-phenyl)
f	793	769	772	CH wag (naphthyl)
	767	744	751	CH wag (t-phenyl)
	751, 755	729, 733	742	CH wag (naphthyl) + CH wag (t-phenyl)
	730	708	717	CC torsion (biphenyl)
	711	690	697	CC torsion (t-phenyl)
	706	685	691 sh	CC torsion (t-phenyl) + CC deformation
	679	658	662	CC torsion (naphthyl) + CC deformation
	661	641	644	CC deformation + CC torsion (biphenyl)
	640	621	624	CC torsion + CC deformation
	632	614	616	CC torsion + CC deformation (t-phenyl)
	619	601	606	CC torsion + CC deformation
	575	558	558	CC torsion (biphenyl + naphthyl)
	550	534	538	CC torsion (biphenyl + naphthyl)
	533	517	521	CC torsion + CC deformation
	528	512	508	CC torsion (biphenyl)
	508	493	497	CC torsion (phenyl) + CC deformation (naphthyl)
	477, 483	463, 469	467	CC torsion + CC deformation + CCN wag
	443	430	439	CC torsion + CC bend (biphenyl + naphthyl)
g	437	424	424	CC torsion (naphthyl)

[a] Harmonic frequencies were scaled by 0.97.

Annealing of NPB thin films

Reflection absorption infrared spectroscopy (RAIRS) is commonly used to study the orientation of nanometric films deposited on a reflecting metal substrate. In RAIRS, the electric field coupling to the vibrational modes of the material is normal to the surface, allowing the determination of average molecular orientation through comparison of relative experimental band intensities. RAIRS is a well established technique and has been used to investigate the effects of thermal annealing for organic semiconductor materials, such as perylene based photoconductors[31–33] and the OLED electron transport material Alq3.[34,35] Recently, Popovic *et al.*[36] used RAIRS to monitor the effect of dopant molecules on the structural changes occurring in NPB thin solid films upon thermal annealing, however detailed discussion was not given. In the present work, with the IR assignments of NPB established by comparison with the DFT calculations, we will discuss the effect of annealing on NPB thin films is greater detail. The RAIRS spectrum of a 200 Å NPB film on a silver mirror was collected at room temperature and then again after annealing at 125 °C for 30 min.

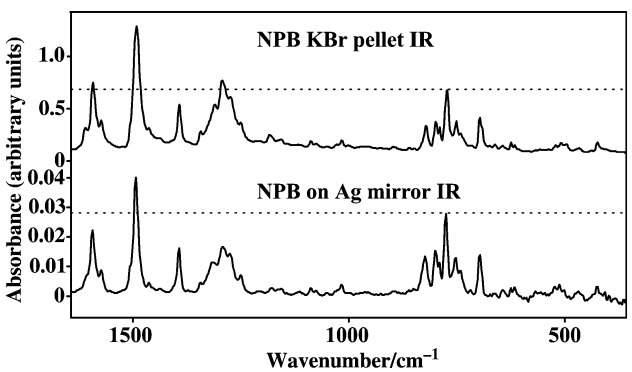

Fig. 3 Experimental pellet IR and thin film refection absorption IR (RAIRS) spectra of NPB for comparison. Note the difference in relative intensities between the two.

The pellet IR spectrum and the room temperature thin film RAIRS spectrum are shown in Fig. 3. Comparison of the relative intensities of the out-of-plane naphthyl CH wag at *ca.* 772 cm^{-1} and the in-plane naphthyl CC stretching vibration observed at *ca.* 1392 cm^{-1}, with transition dipoles perpendicular and parallel to the naphthyl group plane respectively, indicates that on average the naphthyl groups of NPB in the thin film adopt a partially flat orientation relative to the

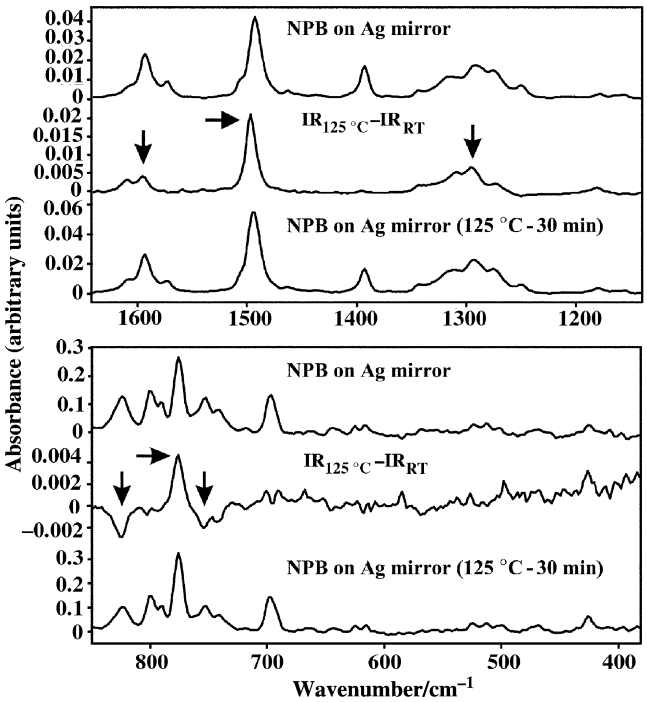

Fig. 4 The RAIRS spectra for a NPB thin film at room temperature and after annealing for 30 min at 125 °C for the in-plane region (top panel) and the out-of-plane region (bottom panel). The IR difference spectrum ($IR_{125\,°C} - IR_{RT}$) is shown indicating the bands of significant intensity change discussed in the text. The ordinate scales of the spectra have been expanded for clarity.

surface. The room temperature and the annealed RAIRS spectra, and the IR difference spectrum ($IR_{125\,°C} - IR_{RT}$) for the NPB thin film are shown in Fig. 4. The ordinate scales of the spectra have been expanded for clarity. The IR difference spectrum in the out-of-plane region (*ca.* 860 cm^{-1} to 400 cm^{-1}) (lower panel)) indicates key differences between the room temperature and annealed spectra. Most significant is the marked increase in intensity of the naphthyl CH wag at *ca.* 772 cm^{-1} and the decrease in intensity of vibrations at *ca.* 821 cm^{-1} and 751 cm^{-1}, assigned to CH waging vibrations involving the phenyl groups, with the latter being mainly localised on the terminal phenyl groups of NPB. These intensity changes suggest that, upon annealing, the naphthyl groups of NPB relax further into a flat average orientation and the phenyl groups tend to prefer a perpendicular conformation with respect to the surface.

Looking to the in-plane region (*ca.* 1150 cm^{-1} to 1650 cm^{-1} (Fig. 4, top panel)) for indications of orientational changes shows that the band at *ca.* 1491 cm^{-1}, assigned to a phenyl CC/CN stretching + CH bending vibration, gains significant intensity upon annealing. Other bands that gain intensity are the CC stretch largely involving the terminal phenyl groups and the phenyl CH bending vibration, at *ca.* 1592 cm^{-1} and 1293 cm^{-1}, respectively. The atomic displacement vectors of the vibrations having the largest increase in intensity upon annealing assigned to the **c** and **f** IR bands are shown in Fig. 5. The reflection absorption IR spectra indicate that upon annealing the NPB films undergo orientational changes consistent with the naphthyl groups being largely parallel to the surface. A potential conformation of NPB on the surface in which the naphthyl groups could be predominantly flat is that where the naphthyl groups are *cis* to each other, as opposed to the gas phase global minimum *trans* conformation. In such a conformation the terminal phenyl groups could be directed up from the surface, which would cause an increase in the intensity of the phenyl CC stretching bands and a decrease in the phenyl CH out-of-plane wags, as is observed in the annealed IR.

Conclusion

The major IR modes of the OLED material NPB have been assigned using the B3LYP/6-31G(d) level of theory. Excellent agreement was found between the experimental IR spectrum and the simulated DFT spectrum, allowing the reliable assignment of observed bands. Reflection absorption IR spectroscopy (RAIRS) was used to investigate orientational changes in NPB thin films upon thermal annealing. With annealing, the naphthyl groups of NPB are found to adopt a predominately flat orientation with respect to the surface.

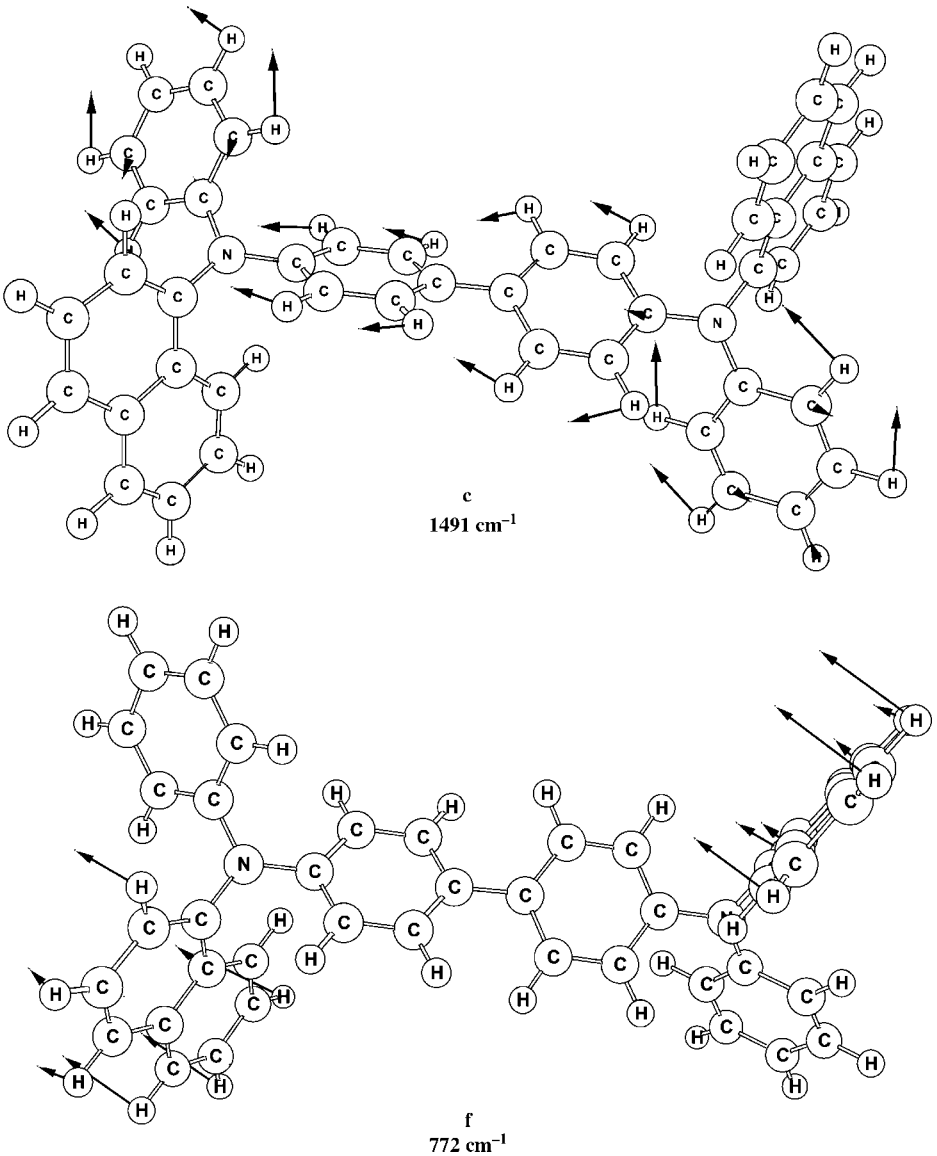

Fig. 5 Normal mode atomic displacement vectors for the **c** and **f** vibrations, which show the largest increase in intensity upon annealing. The experimental frequencies are indicated.

Acknowledgements

HBS and MDH gratefully acknowledge financial support from the National Science Foundation (Grant No. CHE9874005) and a grant for computing resources from NCSA (Grant No. CHE980042N). MDH would also like to thank the Department of Chemistry, Wayne State University for financial support provided by a Wilfred Heller Graduate Fellowship.

References

1 C. W. Tang and S. A. Van Slyke, *Appl. Phys. Lett*., 1987, **51**, 913.
2 J. R. Sheats, H. Antoniadis, M. Hueschen, W. Leonard, J. Miller, R. Moon, D. Roitman and A. Stocking, *Science*, 1996, **273**, 884.
3 J. L. Rothberg and A. J. Lovinger, *J. Mater. Res*., 1996, **11**, 3174.
4 Y. Hamada, *IEEE Trans. Electron Devices*, 1997, **44**, 1208.
5 C. H. Chen and J. Shi, *Coord. Chem. Rev*., 1998, **171**, 161.
6 S. A. Van Slyke, C. H. Chen and C. W. Tang, *Appl. Phys. Lett*., 1996, **15**, 2160.
7 J. McElvain, H. Antoniadis, M. R. Hueschen, J. N. Miller, D. M. Roitman, J. R. Sheets and R. L. Moon, *J. Appl. Phys*., 1996, **80**, 6002.
8 P. E. Burrows, V. Bulovic, S. R. Forrest, L. S. Sapochak, D. M. McCarty and M. E. Thompson, *Appl. Phys. Lett*., 1994, **65**, 2922.
9 H. Aziz and G. Xu, *J. Phys. Chem. B*, 1997, **101**, 4009.
10 F. Papadimitrakipoulos, X. M. Zhang, D. L. Thomsen and K. A. Higginson, *Chem. Mater*., 1996, **8**, 1363.
11 H. Aziz, Z. D. Popovic, N. X. Hu, A. M. Hor and G. Xu, *Science*, 1999, **284**, 1900.
12 L. Do, E. Han, N. Yamamoto and M. Fujihira, *Mol. Cryst. Liq. Cryst*., 1996, **280**, 373.
13 R. Q. Zhang, C. S. Lee and S. T. Lee, *Appl. Phys. Lett*., 1999, **75**, 2418.
14 R. Q. Zhang, C. S. Lee and S. T. Lee, *J. Chem. Phys*., 2000, **112**, 8614.
15 Z. Deng, S. T. Lee, D. P. Webb, Y. C. Chan and W. A. Gambling, *Synth. Met*., 1999, **107**, 107.
16 F. M. Avendano, E. W. Forsythe, Y. Gao and C. W. Tang, *Synth. Met*., 1999, **102**, 910.
17 P. Pulay, in *Modern Electronic Structure Theory*, ed. D. Yarkony, World Scientific, Singapore, 1995, p. 1191.
18 A. P. Scott and L. Radom, *J. Phys. Chem*., 1996, **100**, 16502.
19 M. W. Wong, *Chem. Phys. Lett*., 1996, **256**, 391.
20 M. D. Halls and H. B. Schlegel, *J. Chem. Phys*., 1998, **109**, 10587.
21 M. J. Frisch, G. W. Trucks, H. B. Schlegel, G. E. Scuseria, M. A. Robb, J. R. Cheeseman, V. G. Zakrzewski, J. A. Montgomery, Jr., R. E. Stratmann, J. C. Burant, S. Dapprich, J. M. Millam, A. D. Daniels, K. N. Kudin, M. C. Strain, O. Farkas, J. Tomasi, V. Barone, M. Cossi, R. Cammi, B. Mennucci, C. Pomelli, C. Adamo, S. Clifford, J. Ochterski, G. A. Petersson, P. Y. Ayala, Q. Cui, K. Morokuma, D. K. Malick, A. D. Rabuck, K. Raghavachari, J. B. Foresman, J. Cioslowski, J. V. Ortiz, B. B. Stefanov, G. Liu, A. Liashenko, P. Piskorz, I. Komaromi, R. Gomperts, R. L. Martin, D. J. Fox, T. Keith, M. A. Al-Laham, C. Y. Peng, A. Nanayakkara, C. Gonzalez, M. Challacombe, P. M. W. Gill, B. Johnson, W. Chen. M. W. Wong, J. L. Andres, C. Gonzalez, M. Head-Gordon, E. S. Replogle and J. A. Pople, *GAUSSIAN 98*, Revision A.6, Gaussian, Inc., Pittsburgh, PA, 1998.
22 A. D. Becke, *Can. J. Phys*., 1993, **98**, 5648.
23 C. Lee, W. Yang and R. G. Parr, *Phys. Rev. B*, 1988, **37**, 785.
24 W. J. Hehre, R. Ditchfield and J. A. Pople, *J. Chem. Phys*., 1972, **56**, 2257.
25 P. Botschwina, W. Meyer and A. M. Semkow, *Chem. Phys*., 1976, **15**, 25.
26 G. Fogarasi and P. Pulay, *J. Mol. Struct*., 1977, **39**, 275.
27 P. Pulay, G. Fogarasi, G. Pongor, J. E. Boggs and A. Vargha, *J. Am. Chem. Soc*., 1983, **105**, 7037.
28 Y. N. Panchenko, *Russ. Chem. Bull*., 1996, **45**, 753.
29 M. Ilic, E. Koglin, A. Pohlmeier, H. D. Narres and M. J. Schwuger, *Langmuir*, 2000, **16**, 8946.
30 C. W. Bauschlicher, *Chem. Phys*., 1998, **234**, 87; (http://ccf.arc.nasa.gov/ ~ cbauschl/astro.data2)
31 A. Kam, R. Aroca, J. Duff and C. P. Tripp, *Chem. Mater*., 1998, **10**, 172.
32 A. P. Kam, R. Aroca, J. Duff and C. P. Tripp, *Langmuir*, 2000, **16**, 1185.
33 A. Kam, R. Aroca, J. Duff and C. P. Tripp, *Int. J. Vib. Spectrosc*., 2000, **4**, 2.
34 H. Aziz, Z. Popovic, S. Xie, A. M. Hor, N. X. Hu, C. P. Tripp and G. Xu, *Appl. Phys. Lett*., 1998, **72**, 765.
35 H. Aziz, Z. Popovic, C. P. Tripp, N. X. Hu, A. M. Hor and G. Xu, *Appl. Phys. Lett*., 1998, **72**, 2642.
36 Z. D. Popovic, S. Xie, N. Hu, A. Hor, D. Fork, G. Anderson and C. P. Tripp, *Thin Solid Films*, 2000, **363**, 6.